Supplementary materials to the article: Unified limit cycle amplitude prediction and symmetry breaking analysis of combustion instabilities

1. Decoupling between the plenum and combustion chamber cavities

Combustion systems are often composed of multiple cavities interconnected in various ways. In the present experiments in the MICCA annular combustor, the chamber communicates with the plenum through a collection of injection units arranged in a periodic fashion. The objective of this section is to examine the system modes and show that the chamber modes are essentially decoupled from the plenum and injector modes, so that one may determine the chamber modes by simply considering the chamber geometry and characteristics (sound velocity and boundary conditions). In other words, there is no need to take into account the injector-port acoustics and the coupling with the plenum to determine the chamber eigenmodes and eigenfrequencies. The modes and their frequencies can be calculated analytically in a framework derived by Evesque & Polifke (2002), Stow & Dowling (2003) or Bauerheim *et al.* (2014). It is also possible to use a Helmholtz solver (Laera *et al.* (2017)) but this numerical method provides a lesser degree of physical insight on the respective contributions of the different cavities to the acoustics of the system than the analytical approach.

The following calculation is based on the framework proposed by Evesque & Polifke (2002). It relies on an idealized representation of the MICCA annular combustor, in which the annular plenum and combustion chamber are linked by 16 injection tubes, terminated by the injection units, as shown in Fig. 1. The plenum backplane is at $x = -l_1$, the injection tube inlet and outlet at $x = 0$ and $x = l_2$, and the combustion chamber exhaust at $x = l_3$.

The rotational symmetry of the problem allows to only consider one sector of the annular combustor for the calculations. As in Evesque & Polifke (2002), the following hypothesis are made:

- The flow perturbations are described in the axial and circumferential directions
- The radial dependence of the physical variables is omitted
- Acoustic waves are standing in the azimuthal direction

The pressure field is described using Riemann invariants, f^n and g^n, respectively travelling in the downstream and upstream directions:

$$f^n(x) = F^n e^{ik_x^n x}, \quad g^n(x) = G^n e^{-ik_x^n x} \tag{1.1}$$

where n designates the axial modal number, $k_x^n = [(\omega/c)^2 - (k_y^m)^2]^{1/2}$ is the axial wavenumber, $k_y^m = m/R$ defines the circumferential wavenumber and $\kappa_n = k_x^n/k$, compares the axial wavenumber to the total wavenumber $k = \omega/c$ and describes the inclination of the wavefront with respect to the x axis. The quantities related to the plenum, injection channel

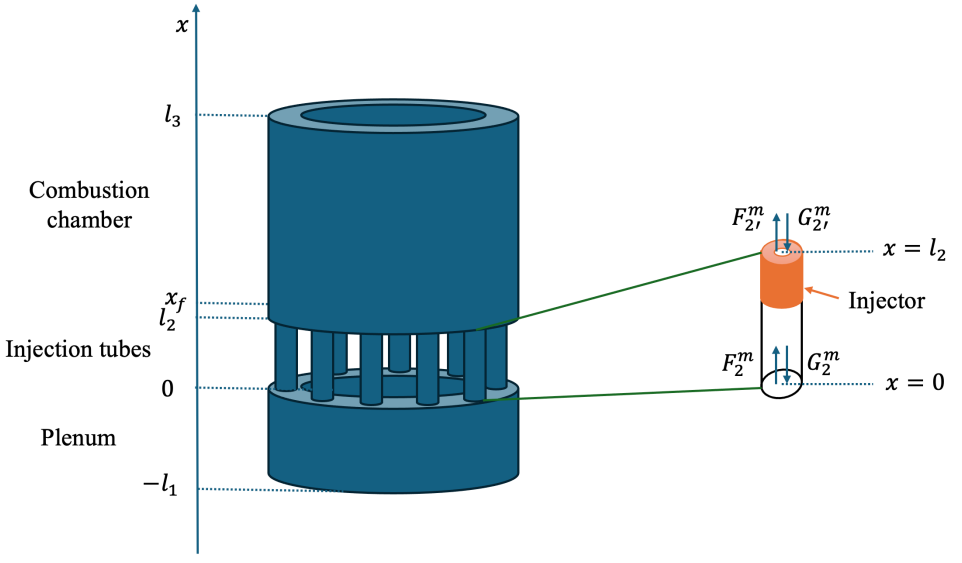

Figure 1: Idealized representation of an annular combustor and zoom on an injection tube.

and chamber are respectively denoted with a subscript "1", "2" and "3". Using the Riemann invariants defined in Eqs. 1.1, the acoustic pressure and velocity in the plenum, p'_1 and v'_1, read:

$$p'_1 = \cos(\frac{my}{R_1})(F_1^n e^{ik_{x1}^n x} + G_1^n e^{-ik_{x1}^n x})e^{-i\omega t} \tag{1.2}$$

$$u'_1 = \frac{1}{\rho_1 c_1}\cos(\frac{my}{R_1})(F_1^n e^{ik_{x1}^n x} - G_1^m e^{-ik_{x1}^n x})\kappa_1^m e^{-i\omega t} \tag{1.3}$$

where R_1 is the mean radius of the annular plenum. In a similar fashion, one has in the chamber:

$$p'_3 = \cos(\frac{my}{R_3})(F_3^n e^{ik_{x3}^n x} + G_3^n e^{-ik_{x3}^n x})e^{-i\omega t} \tag{1.4}$$

$$u'_3 = \frac{1}{\rho_3 c_3}\cos(\frac{my}{R_3})(F_3^n e^{ik_{x3}^n x} - G_3^n e^{-ik_{x3}^n x})\kappa_3^m e^{-i\omega t} \tag{1.5}$$

where R_3 designates the mean radius of the annular chamber. The injection tubes are quite narrow and the waves may be considered to be planar. The link between the acoustic waves at the inlet (F_2^n and G_2^n) and at the outlet ($F_{2'}^n$ and $G_{2'}^n$) of this element may then be obtained by considering the transfer matrices $\mathbf{T}$ of the injection units, as sketched in Fig. 1. As the injector does not occupy the whole length of the injection tube, the link between the acoustic variables at the inlet and outlet of the tube has to be determined using a network of transfer matrices, as shown in Fig. 2:

$$\begin{bmatrix} p'_d/\rho c \\ v'_d \end{bmatrix} = \mathbf{M}\begin{bmatrix} p'_a/\rho c \\ v'_a \end{bmatrix} \tag{1.6}$$

with

$$\mathbf{M} = \begin{bmatrix} M_{11} & M_{12} \\ M_{21} & M_{22} \end{bmatrix} = \begin{bmatrix} T_{11} & T_{12} \\ T_{21} & T_{22} \end{bmatrix}\begin{bmatrix} 1 & 0 \\ 0 & S_b/S_c \end{bmatrix}\begin{bmatrix} \cos(k_2 l_b) & i\sin(k_2 l_b) \\ i\sin(k_2 l_b) & \cos(k_2 l_b) \end{bmatrix} \tag{1.7}$$

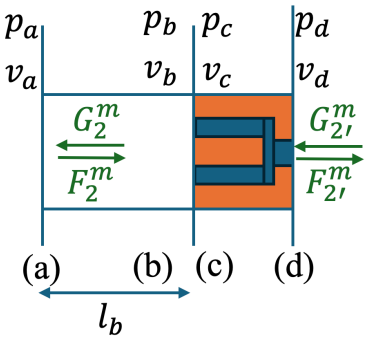

Figure 2: Injection tube model and link between the upstream and downstream acoustic variables.

The acoustic pressure and velocity at the outlet of the injection tube, p'_d and v'_d, read:

$$\frac{p'_d}{\rho c} = M_{11}\frac{p'_a}{\rho c} + M_{12}v'_a, \quad v'_d = M_{21}\frac{p'_a}{\rho c} + M_{22}v'_a \tag{1.8}$$

which can be rewritten in terms of Riemann invariants as

$$F^n_{2'}e^{ik^n_2 l_2} + G^n_{2'}e^{-ik^n_2 l_2} = M_{11}(F^n_2 + G^n_2) + M_{12}(F^n_2 - G^n_2) \tag{1.9}$$

$$F^n_{2'}e^{ik^n_2 l_2} - G^n_{2'}e^{-ik^n_2 l_2} = M_{21}(F^n_2 + G^n_2) + M_{22}(F^n_2 - G^n_2) \tag{1.10}$$

the subscript $2'$ designating quantities at the outlet of the injection tube and the subscript 2, at the inlet.

The boundary conditions have now to be written to find the dispersion relation to solve to find the eigenmodes of the MICCA combustor. The system of equations reads:

- Open end at $x = l_3$:

$$F^n_3 e^{ik^n_{x3} l_3} + G^n_3 e^{-ik^n_{x3} l_3} = 0 \tag{1.11}$$

- Pressure and volume flow rate continuity at $x = l_2$:

$$F^n_{2'}e^{ik^n_{x2} l_2} + G^n_{2'}e^{-ik^n_{x2} l_2} = F^n_3 e^{ik^n_{x3} l_2} + G^n_3 e^{-ik^n_{x3} l_2} \tag{1.12}$$

$$\alpha_3(F^n_{2'}e^{ik^n_{x2} l_2} - G^n_{2'}e^{-ik^n_{x2} l_2}) = (F^n_3 e^{ik^n_{x3} l_2} - G^n_3 e^{-ik^n_{x3} l_2})\kappa^n_3 \tag{1.13}$$

- Connection between the injection tube inlet and outlet

$$F^n_{2'}e^{ik^n_2 l_2} + G^n_{2'}e^{-ik^n_2 l_2} = M_{11}(F^n_2 + G^n_2) + M_{12}(F^n_2 - G^n_2) \tag{1.14}$$

$$F^n_{2'}e^{ik^n_2 l_2} - G^n_{2'}e^{-ik^n_2 l_2} = M_{21}(F^n_2 + G^n_2) + M_{22}(F^n_2 - G^n_2) \tag{1.15}$$

- Pressure and volume flow rate continuity at $x = 0$:

$$F^n_1 + G^n_1 = F^n_2 + G^n_2 \tag{1.16}$$

$$\alpha_1\kappa^n_1(F^n_1 - G^n_1) = F^n_2 - G^n_2 \tag{1.17}$$

- Closed end at $x = -l_1$:

$$F^n_1 e^{-ik^n_{x1} l_1} - G^n_1 e^{ik^n_{x1} l_1} = 0 \tag{1.18}$$

In these equations, α_1 and α_3 can be identified as "acoustic coupling indices" (Schuller *et al.* (2012)) between the different cavities forming the MICCA combustor:

$$\alpha_1 = \frac{S_1}{S_2}\frac{\rho_2 c_2}{\rho_1 c_1}, \quad \alpha_3 = \frac{S_{2'}}{S_3}\frac{\rho_3 c_3}{\rho_{2'} c_{2'}} \approx \frac{S_{2'}}{S_3}\left(\frac{T_{2'}}{T_3}\right)^{1/2} \tag{1.19}$$

Plenum (1)	Section of a sector: $S_1 = 34.4$ cm^2, $T_1 = T_u$
Injection tube (2)	Section of a tube: $S_2 = 12.6$ cm^2, $T_2 = T_u$
Injector outlet (2')	Section at the injector outlet: $S_{2'} = 0.5$ cm^2, $T_{2'} = T_u$
Combustion chamber (3)	Section of a sector: $S_3 = 34.4$ cm^2, $T_3 = T_b$

Table 1: Sections and temperatures in the different cavities. $T_u = 300$ K corresponds to the temperature in the fresh gases and $T_b = 1400$ K to that in the burnt gases.

The sections and temperatures in the different cavities, enabling the evaluation of these acoustic coupling indices are reported in Tab. 1. The system formed by Eqs. 1.11 to 1.18 can then be written in the form $\mathbf{NX} = 0$, where

$$\mathbf{N} = \begin{bmatrix} e^{-ik^n_{x1}l_1} & -e^{ik^n_{x1}l_1} & 0 & 0 & 0 & 0 & 0 & 0 \\ \alpha_1\kappa^n_1 & -\alpha_1\kappa^n_1 & -1 & 1 & 0 & 0 & 0 & 0 \\ 1 & 1 & -1 & -1 & 0 & 0 & 0 & 0 \\ 0 & 0 & \mathcal{M}_1 & \mathcal{M}_2 & -e^{ik^n_{x2}l_2} & -e^{-ik^n_{x2}l_2} & 0 & 0 \\ 0 & 0 & \mathcal{M}_3 & \mathcal{M}_4 & -e^{ik^n_{x2}l_2} & e^{-ik^n_{x2}l_2} & 0 & 0 \\ 0 & 0 & 0 & 0 & \alpha_3 e^{ik^n_{x2}l_2} & -\alpha_3 e^{-ik^n_{x2}l_2} & -\kappa^n_3 e^{ik^n_{x3}l_2} & \kappa^n_3 e^{-ik^n_{x3}l_2} \\ 0 & 0 & 0 & 0 & e^{ik^n_{x2}l_2} & e^{-ik^n_{x2}l_2} & -e^{ik^n_{x3}l_2} & -e^{-ik^n_{x3}l_2} \\ 0 & 0 & 0 & 0 & 0 & 0 & e^{ik^n_{x3}l_3} & e^{-ik^n_{x3}l_3} \end{bmatrix} \tag{1.20}$$

where $\mathcal{M}_1 = M_{11} + M_{12}$, $\mathcal{M}_2 = M_{11} - M_{12}$, $\mathcal{M}_3 = M_{21} + M_{22}$ and $\mathcal{M}_4 = M_{21} + M_{22}$. and

$$\mathbf{X}^T = \begin{bmatrix} F^n_1 & G^n_1 & F^n_2 & G^n_2 & F^n_{2'} & G^n_{2'} & F^n_3 & G^n_3 \end{bmatrix} \tag{1.21}$$

The system has a non-zero solution if $\det(\mathbf{N}) = 0$. The latter equation constitutes the dispersion relation. Expanding the determinant of the system with respect to the last column and then the last row, one gets:

$$\det(\mathbf{N}) = 2\det(\mathbf{D})\kappa^n_3 \cos(\kappa^n_{x3}(l_3 - l_2)) + 2i\det(\mathbf{C})\sin(\kappa^n_{x3}(l_3 - l_2)) \tag{1.22}$$

with

$$\det(\mathbf{C}) = \begin{vmatrix} e^{-ik^n_{x1}l_1} & -e^{ik^n_{x1}l_1} & 0 & 0 & 0 & 0 \\ \alpha_1\kappa^n_1 & -\alpha_1\kappa^n_1 & -1 & 1 & 0 & 0 \\ 1 & 1 & -1 & -1 & 0 & 0 \\ 0 & 0 & \mathcal{M}_1 & \mathcal{M}_2 & -e^{ik^n_{x2}l_2} & -e^{-ik^n_{x2}l_2} \\ 0 & 0 & \mathcal{M}_3 & \mathcal{M}_4 & -e^{ik^n_{x2}l_2} & e^{-ik^n_{x2}l_2} \\ 0 & 0 & 0 & 0 & \alpha_3 e^{ik^n_{x2}l_2} & -\alpha_3 e^{-ik^n_{x2}l_2} \end{vmatrix} \tag{1.23}$$

and

$$\det(\mathbf{D}) = \begin{vmatrix} e^{-ik^n_{x1}l_1} & -e^{ik^n_{x1}l_1} & 0 & 0 & 0 & 0 \\ \alpha_1\kappa^n_1 & -\alpha_1\kappa^n_1 & -1 & 1 & 0 & 0 \\ 1 & 1 & -1 & -1 & 0 & 0 \\ 0 & 0 & \mathcal{M}_1 & \mathcal{M}_2 & -e^{ik^n_{x2}l_2} & -e^{-ik^n_{x2}l_2} \\ 0 & 0 & \mathcal{M}_3 & \mathcal{M}_4 & -e^{ik^n_{x2}l_2} & e^{-ik^n_{x2}l_2} \\ 0 & 0 & 0 & 0 & e^{ik^n_{x2}l_2} & e^{-ik^n_{x2}l_2} \end{vmatrix} \tag{1.24}$$

One can see that $\det(\mathbf{C})$ reflects the coupling between the injection tube filled with fresh gases with the combustion chamber filled with burnt products, through the acoustic coupling index α_3. The modes associated with the plenum and injection tube appear in $\det(\mathbf{D})$.

One can notice that $\det(\mathbf{C}) \propto \alpha_3$. In the MICCA configuration, one gets, using Tab. 1,

$\alpha_3 \approx 0.003$. For the frequency range of interest ([700-1500 Hz]), a rapid estimation gives values for κ_3^n between 0.2 and 0.8, hence at least two orders of magnitude higher than α_3.

The second term on the right-hand side of Eq. 1.22 can then be assumed to be small compared to the first, and one may write:

$$\det(\mathbf{N}) \approx 2\det(\mathbf{D})\kappa_3^n \cos(\kappa_{x3}^n(l_3 - l_2)) \tag{1.25}$$

Thus, $\det(\mathbf{N}) = 0$ if :

- $\cos(\kappa_{x3}^n(l_3 - l_2)) = 0$, which corresponds to the chamber modes, with an open-end outlet and a rigid backplane.
- or $\det(\mathbf{D}) = 0$, corresponding to the modes of the plenum and injection tube, which are a function of the combustor geometrical parameters and the injection unit transfer matrix coefficients.

Solving $\cos(\kappa_{x3}^n(l_3 - l_2)) = 0$, one gets:

$$\kappa_{x3}^n(l_3 - l_2) = \frac{\pi}{2}(2n - 1) \tag{1.26}$$

Using the definition of the axial wavenumber, one may write:

$$(\frac{\omega}{c})^2 = (k_y^m)^2 + (\kappa_{x3}^n)^2 \tag{1.27}$$

which lead to eigenfrequencies of the form :

$$f_{m,n} = c\left[\left(\frac{m}{2\pi R_3}\right)^2 + \left(\frac{(2n-1)}{4(l_3 - l_2)}\right)^2\right]^{1/2} \tag{1.28}$$

Using $2\pi R_3 = \mathcal{P}_a$ and $l_3 - l_2 = l'$ one obtains

$$f_{m,n} = c\left[\left(\frac{m}{\mathcal{P}_a}\right)^2 + \left(\frac{(2n-1)}{4l'}\right)^2\right]^{1/2} \tag{1.29}$$

which becomes Eq. (2.2) of the article when on sets $m = 1$ and $n = 1$. This indicates that the modes of the MICCA combustion chamber are not influenced by the injection units, injection tubes and plenum.

The possibility of frequency veering is excluded because the 1A1L chamber mode does not match one of the plenum modes.

2. Effects of frequency on the pressure-based FDF data

Contrary to a forced experiment, the method used in this work to obtain FDF data in the annular combustor MICCA relies on the ability to obtain a well-defined standing mode with a controlled nodal line position through injector staging. The frequency of the self-sustained oscillations is thus imposed by the staging pattern. One hence needs to verify that the data is not biased by these variations in self-sustained oscillation frequencies.

The modulation frequency that defines flame oscillations in each staging configuration results from the closed loop interaction between the acoustics of the MICCA combustor and the flames, and is thus imposed by the coupling and is therefore dependent on the staging pattern. As shown in Alhaffar *et al.* (2024), the self-sustained oscillation frequencies of the seven injector configurations used for pressure-based FDF determination vary between 774 and 802 Hz. Although this range of frequency variation is limited, one needs to check that these changes in self-sustained oscillation frequencies do not lead to differences in the flame response. In Fig. 3, the points are colored by the frequency value. There is no visible

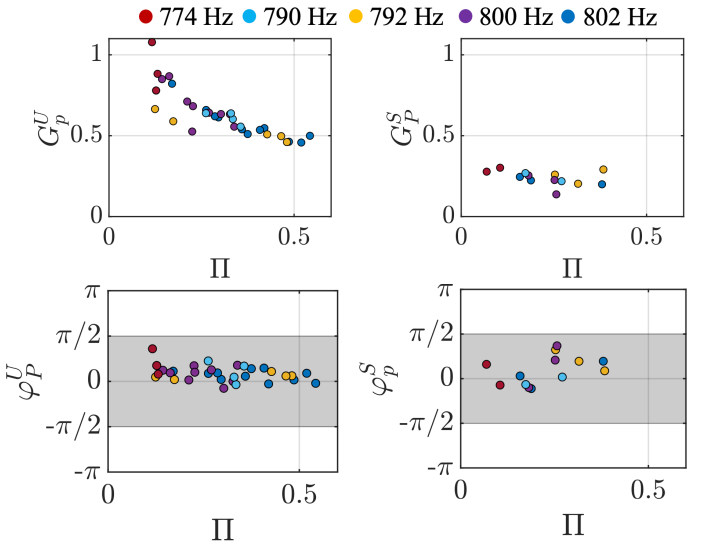

Figure 3: Pressure-based FDF gain (top) and phase (phase) for injectors U (left) and S (right), colored by the instability frequency.

trend with respect to the relatively small frequency variations and one may conclude that the frequency shifts do not affect the collected flame dynamics data.

REFERENCES

Alhaffar A., Latour V., Patat C., Durox D., Renaud A., Blaisot J.-B., Candel S. and Baillot F. 2024 Comparison of pressure-based flame describing functions measured in an annular combustor under self-sustained oscillations and in an externally modulated linear combustor, *Proc. Combust. Inst.*, **40**, 105249.

Bauerheim M., Parmentier J.-F., Salas P., Nicoud F. and Poinsot T. 2014 An analytical model for azimuthal thermoacoustic modes in an annular chamber fed by an annular plenum, *Combust. Flame*, **161**, pp. 1374-1389.

Evesque S. and Polifke W. 2002 Low-order acoustic modelling for annular combustors: Validation and inclusion of modal coupling, *In Proc. ASME Turbo Expo. 2002*, Paper GT2002-30064.

Laera D., Prieur K., Durox D., Schuller T., Camporeale S.M. and Candel S. 2017 Impact of heat release distribution on the spinning modes of an annular combustor with multiple matrix burners, *ASME J. Eng. Gas Turbines Power*, **139(5)**, p. 51505.

Schuller T., Durox D., Palies P, and Candel S. 2012 Acoustic decoupling of longitudinal modes in generic combustion systems, *Combust. Flame*, **159**, pp. 1921-1931.

Stow S.R. and Dowling A.P. 2003 Modelling of circumferential modal coupling due to Helmholtz resonators, *In Proc. ASME Turbo Expo 2003*, Paper GT2003-38168.